Towards Construction 4.0 Spraying Technologies: Development of an Automated Modular Spraying System (AMSS) for Varying-Viscosity Coating Applications

Rajesh Ranjan Nayak[1], Masoud Shakoorianfard[1], Christian Richter[1], and Frank Will[1]

[1]Chair of Construction Machinery, Dresden University of Technology, Germany
[rajesh_ranjan.nayak, masoud.shakoorianfard, christian.richter1, frank.will]@tu-dresden.de

Abstract –

As the construction industry transitions toward Construction 4.0, there is an increasing demand for automated technologies to replace labour-intensive manual coating processes at construction sites. Traditional spraying systems are often limited to single-mode operation and manual control, making them insufficient for the automated application of diverse material properties found on modern jobsites. This work addresses three linked research challenges: integrating multiple spray principles within one carrier-agnostic spray head, maintaining control of critical process parameters across material-dependent behaviour, and establishing a pathway toward rheology-aware adaptation. The implemented AMSS addresses these challenges at a first stage through software-selectable multi-mode spraying and perception-guided pose control, with results showing stable sprayability across a wide apparent-viscosity range and mode-dependent modulation of plume width without hardware replacement.

AMSS combines a modular spray head for Airless, AirCoat, and Airmix modes with ROS 2-based control, embedded real-time actuation, and ToF-based stand-off and surface-orientation sensing. Experimental validation across multiple materials used high-speed imaging and pixel-based deposited-surface metrics to assess sprayability, plume stability, control over the deposited spray footprint, and edge overspray. The results indicate stable multi-material spraying and mode-dependent control of both plume behaviour and deposited-surface behaviour, supporting scalable automated coating applications.

Keywords –

Construction 4.0; spray; carrier-agnostic; AMSS; multi-mode spraying; embedded real-time actuation; ToF; surface-orientation sensing; pixel-based; spray footprint

1 Introduction

The construction industry is progressing toward Construction 4.0, intensifying efforts to improve productivity, quality, and safety through automation, digitalization, and cyber-physical systems [1]. While significant progress has been achieved in planning, prefabrication, and industrialized construction, many on-site finishing operations remain labour-intensive and highly variable [1].

Despite these expectations, coating and painting still do not adapt to the automated site processes and continue to exhibit low productivity, inconsistent quality, and elevated health and safety risks relative to other Construction 4.0 domains. [2, 3, 4]. Across application domains, mechanization alone has not eliminated variability: in shotcrete, mechanized delivery is common, yet thickness and quality remain strongly dependent on nozzleman skill; empirical thickness control encourages overspray to avoid under-thickness, increasing waste, variability, and rework [2,5]. Similar issues are reported for waterproofing and coating applications, motivating dedicated spraying robots designed to deliver uniform layers and stable quality [6]. For interior and exterior wall finishing, robotic spraying systems have been proposed to address low on-site efficiency and high labour costs, with reported cost savings exceeding 30% compared to manual methods [3,7,8]; experimental and field studies further report that automated systems can meet or exceed standard quality requirements while achieving consistent layer thickness and improved surface finish [10].

Automation is additionally motivated by occupational safety and labour shortages. Spraying exposes workers to dust, volatile organic compounds (VOCs), and toxic agents, and shotcrete rebound and airborne particles are associated with serious respiratory diseases [2,11]. Automated spray-painting systems can remove operators from hazardous environments, reducing chemical exposure and improving ergonomics, while recent robotic solutions explicitly target reductions in falls from height and inhalation of hazardous fumes [4].

Regulatory and sustainability pressures further constrain site practice. Tightening requirements impose non-negotiable limits on emissions, worker protection, and resource efficiency [11], and, in practice, shift material portfolios toward water-based, low-emission products. A central technical barrier to robust automation is the "viscosity challenge": construction coatings exhibit wide and time-varying rheological behaviour, including (1) variability in viscosity, (2) shear-thinning, thixotropy, (3) particle content, and (4) setting behaviour across batches and during application, which can degrade spray fidelity and lead to unstable jets, sagging or uneven deposition, excessive overspray, and nozzle clogging [12]. As a result, systems designed for a single material or narrow class often fail to transfer across the broad range of construction coatings demanded on site, strengthening the case for modular automated spraying concepts that support multi-material processing with high reproducibility and reduced environmental impact [14,15].

This paper addresses these challenges by presenting the development direction of an Automated Modular Spraying System (AMSS) aimed at carrier-agnostic robotic deployment and multi-material capability. As illustrated in Fig. 1, unlike many existing robotic sprayers that are implemented as fixed, single-purpose units tied to a specific carrier or a single atomization principle, AMSS is designed as a carrier-agnostic modular end-effector that integrates airless, aircoat, and airmix operation within one spray head. Its distinction therefore lies not only in modularity, but in enabling different material classes and viscosities to be processed through software-selectable spray modes without requiring carrier-specific redesign or hardware replacement. The central premise is that construction, site-ready spraying automation requires the integration of (1) adaptable spray hardware supporting multiple atomization modes, (2) systematic parameterization that accommodates material variability, and (3) sensing-to-actuation loops that enable stable, repeatable application under construction-relevant conditions.

The organization of this paper is as follows: Section 2 provides the state of the art for construction material application with its gaps. Section 3 explains the development of the AMSS and communication architecture. Section 4 shows the implementation of AMSS and its outcomes. Finally, the conclusion and future scope are discussed in Section 5.

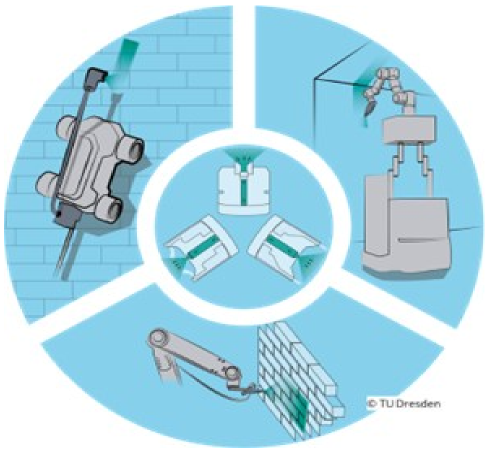

Figure 1. Schematic illustration of the AMSS

2 State of the Art

2.1 Spraying techniques

Industrial spraying technologies provide a reference framework for construction-oriented systems because they rely on well-defined atomization mechanisms and controlled material delivery. Air-based atomization approaches (e.g., Airmix and related variants) can achieve fine atomization but typically introduce greater overspray and aerosol formation, while transfer efficiency depends not only on pressure but also on airflow characteristics and equipment configuration [16]. In airless spraying, atomization occurs through high material pressure without additional air, enabling high area coverage and applicability to higher-viscosity materials, although atomization is generally coarser and fan-width adjustment often requires nozzle changes [17]. Air-assisted airless (AirCoat) adds compressed-air support to stabilize the jet and reduce banding, while airmix remains relevant for highly viscous, particle-containing materials such as putty or plaster [15].

2.2 Construction spraying practice and implications for AMSS design

Construction spraying transfers industrial atomization principles into open, unstructured, and large-scale site environments, where process conditions are less controlled and material variability is substantially higher. As a result, current construction spraying remains predominantly manual or semi-mechanized and frequently lacks modularity: spray heads are often rigidly integrated into fixed carriers, limiting versatility and increasing acquisition costs. Typical applications include façade painting and floor and roof coatings, as well as sealing slurries, plasters, insulating compounds, and thick bitumen-based protective or decorative coatings.

Qualification rates as low as 70% have been reported under manual or poorly controlled spraying conditions [16]. Although airless spraying can improve transfer efficiency compared to airmix approaches, high flow rates still drive wastage when parameters are not systematically optimized [15]. Semi-automated solutions can increase throughput, with mortar application systems reporting 30 m²/h versus 5 m²/h manually [18]; however, substantial human intervention often remains necessary for posture adjustment and quality verification, keeping productivity and quality strongly influenced by operator decisions [7].

Accordingly, research has increasingly focused on robotic and automated spraying systems. Representative platforms such as Pictobot (interior painting) and OutoBot (façade work) aim to reduce manual labour and improve consistency [7,8], while related work in robotic shotcrete and generative manufacturing highlights surface tolerance and process robustness as persistent challenges [19]. In parallel, enabling technologies for perception and planning have advanced. This includes, among others, adoption of DGPS as well as machine vision (through LiDAR sensors and depth cameras) for localization, environment recognition, adaptive trajectory generation, and feedback for positioning and collision avoidance [20]. BIM can provide a priori geometry and support deployment, yet it does not resolve core process-level limitations [4]. Similarly, Human-Robot Collaboration (HRC) concepts and AI-based inspection (e.g., enhanced YOLOv8 variants) improve workflow integration and defect detection but primarily address geometric uncertainty and inspection, rather than the coupling between material behaviour and spray-process stability [3].

The dominant unresolved limitation is the absence of integrated, rheology-aware sensing-to-actuation loops capable of maintaining spray fidelity across diverse construction materials. Variations in viscosity, thixotropy, curing dynamics, or particle size can induce boundary-layer separation, sagging, uneven deposition, and nozzle clogging [13]. Moreover, many systems remain specialized to a single material class and tightly couple spray heads to carriers, restricting reuse and economic viability. Closed-loop control approaches that derive material-specific process windows and regulate them via real-time surface-quality feedback remain scarce, leaving overspray, banding patterns, and inconsistent surface quality unresolved during material switching [3].

These gaps motivate the development of modular, multi-material end-effector concepts that integrate multiple spray modes with automated control, providing the basis for the AMSS direction presented in this work (Fig. 1). In this context, the key research challenges are the integration of multiple spraying techniques within a single modular spray head, the maintenance of repeatable control over critical process parameters (pressure, traverse speed, and stand-off distance) across material-dependent behaviour, and the establishment of a pathway toward rheology-aware real-time parameter adjustment.

3 Development of the Automated Modular Spraying System (AMSS)

The development of the AMSS follows a system-oriented approach that integrates mechanical actuation, perception, and software control into a unified robotic spraying platform. The primary objective is to enable automated multi-material spraying under varying process parameters, while adapting the atomization principle to the material and application context (e.g., airless, air-assisted, airmix). The AMSS targets reproducible spray quality with reduced overspray, achieved through the combination of (1) a modular, carrier-agnostic spray end-effector, (2) a real-time perception pipeline, and (3) a distributed ROS 2-based control architecture.

3.1 Mechanical Design and Actuation

At the core of the AMSS is a modular spray head designed as a carrier-agnostic robotic end effector. The mechanical design layout supports multiple spraying techniques, including airless, air-assisted airless (AirCoat), external airmix, and hybrid combinations through coordinated routing and switching of material and air paths. Coating material is supplied from an external pump through a heated hose, enabling controlled pressure and temperature to accommodate different material rheology.

High-pressure material flow and air supply are controlled via industrial-grade valves. Specifically for the material flow, pneumatically actuated gate valves were selected over hydraulic or electrically actuated alternatives to ensure reliable switching, while keeping the valve core largely isolated from direct wear caused by abrasive particles common in construction materials. This design choice enables sharp spray triggering and clean transitions between spraying and repositioning phases. In addition, proportional valves regulate air pressure and volumetric flow, allowing continuous adjustment of atomization intensity and air support without hardware replacement. Fig. 2 summarizes the AMSS system architecture, highlighting the coupled material–air routing and valve-actuated parameter control used to switch between airless, AirCoat, and airmix modes.

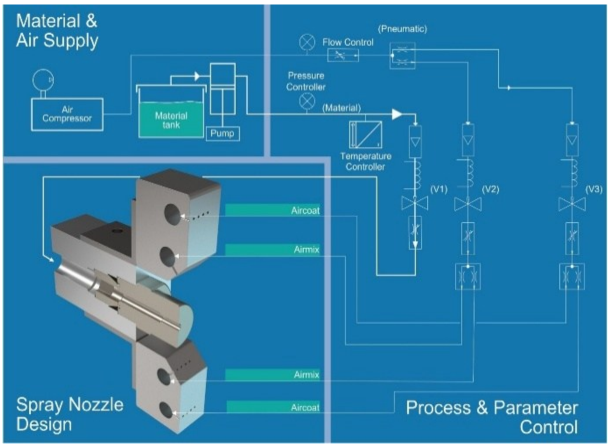

Figure 2. AMSS system architecture overview

Valve actuation and interlock logic are implemented on an Arduino Portenta Machine Control operating in a PLC-like role with a 4-millisecond control period (250 Hz), providing deterministic timing for critical switching under high-pressure conditions. This separation of low-level real-time actuation from high-level planning and perception simplifies integration with different robotic carriers and ensures predictable spray onset or offset independent of the robot's motion planner. The mechanical design further minimizes dead volume in the material path to reduce response delay and hysteresis, which is particularly relevant for viscous and thixotropic construction materials. Table 1 summarizes the predefined valve state configurations used for spray-mode selection and repeatable mode switching.

Table 1 Valve control and spray modes

Spraying Mode	Material (V1)	Airmix (V2)	Aircoat (V3)
Airless	Open	Close	Close
Aircoat	Open	Close	Open
Airmix	Open	Open	Close
Airmix + Aircoat	Open	Open	Open
System Off	Close	Any	Any

3.2 Perception and Spatial Mapping

Reliable robotic spraying in construction environments requires low-latency estimation of stand-off distance and local surface orientation directly at the end-effector. Global point-cloud reconstruction, RANSAC plane fitting, or iterative optimization are often computationally expensive and sensitive to outliers, making them unsuitable for real-time, end-effector-mounted operation. To achieve robust local perception, the AMSS adopts a depth-based sensing strategy utilizing a Luxonis OAK ToF camera in conjunction with the Patch-Based Local Planar Approximation (PBLPA) method. The overall perception-to-action workflow is summarized in Fig. 3.

PBLPA treats the depth image as a discrete scalar field and estimates local surface orientation through differential depth gradients rather than explicit 3D reconstruction. Four median filtered depth patches are sampled symmetrically around the optical axis, $\boldsymbol{z}_{\{tl\}}, \boldsymbol{z}_{\{tr\}}, \boldsymbol{z}_{\{bl\}}, and\ \boldsymbol{z}_{\{br\}}$. Finite differences across opposing patch pairs yield approximations of the local depth gradients:

$$\Delta z_x = \frac{((z_{tr} + z_{br}) - (z_{tl} + z_{bl}))}{2} \tag{1}$$

$$\Delta z_y = \frac{((z_{bl} + z_{br}) - (z_{tl} + z_{tr}))}{2} \tag{2}$$

To convert these gradients into metric space, the effective pixel displacement is scaled using the camera intrinsic focal lengths f_x , f_y and the mean standoff distance z. For a patch sampling radius r, the metric displacements are

$$\Delta x = \left(\frac{r}{f_x}\right) z \tag{3}$$

$$\Delta y = \left(\frac{r}{f_y}\right) z \tag{4}$$

The resulting surface tilt angles, corresponding to roll and pitch of the substrate relative to the spray head, are computed as

$$\theta_x = \arctan\left(\frac{\Delta z_x}{\Delta x}\right) \tag{5}$$

$$\theta_z = \arctan\left(\frac{\Delta z_z}{\Delta y}\right) \tag{6}$$

This formulation implicitly defines a local surface normal consistent with differential geometry-based representations used in robotic movement perception. To mitigate frame to frame jitter common in stereo and ToF depth sensors, the estimated angles are smoothed using an exponential moving average filter:

$$\theta(t) = \alpha\bar{\theta}(t) + (1 - \alpha)\theta(t-1) \tag{7}$$

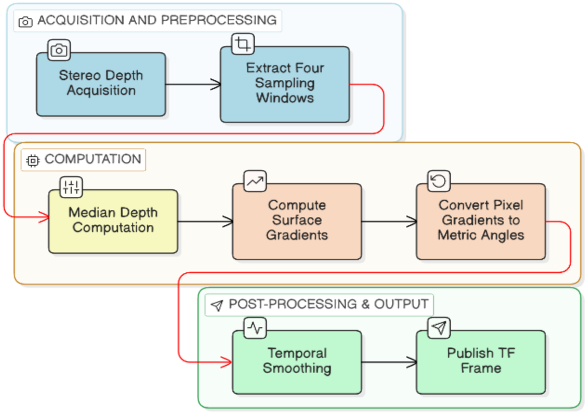

Figure 3. Perception-to-action workflow

Where α denotes the smoothing factor. The filtered orientation and distance define a local surface pose that is broadcasted as a dynamic frame F_s relative to the camera frame F_c. Representing the target surface as a live coordinate frame enables downstream modules to treat the substrate as a moving reference rather than a static plane, supporting continuous correction of nozzle orientation and stand-off distance during execution.

3.3 ROS 2 communication architecture

AMSS is organized as a state-based workflow coupling perception, parameter control, and deterministic actuation. The operational sequence is illustrated in Fig. 4 and is executed as a coordinated ROS 2 pipeline, in which each stage exposes clear interfaces to the next.

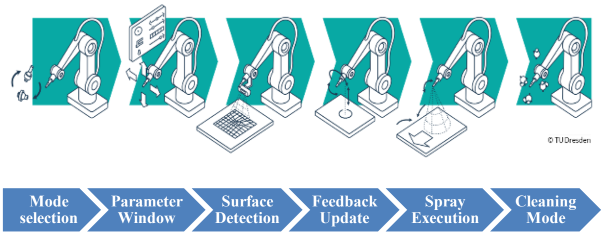

Figure 4. AMSS operational workflow overview

- Mode selection → Parameter window

Each spraying task begins with selecting the intended coating material and application objective. Based on this selection, AMSS activates the corresponding spray mode (e.g., airless, AirCoat, airmix, or hybrid) and loads a predefined valve-state configuration (Table 1). In parallel, a parameter window is initialized, defining admissible ranges for key process variables (e.g., material pressure, temperature, and air pressure). At the current stage, this should be understood as structured parameterization with perception-guided execution rather than fully adaptive control, since spray mode selection and admissible parameter windows are predefined. Real-time rheology inference and plume-driven adaptive mode switching are not yet implemented and remain part of future development.

- Surface detection → Feedback update

During motion, the end-effector-mounted ToF perception stack estimates stand-off distance and local surface orientation (Section 3.2). The resulting surface pose is published as a dynamic TF2 frame, enabling downstream modules to treat the target as a moving reference. The controller then performs a feedback update by computing pose corrections required to maintain near normal incidence and the desired stand-off distance.

- Spray execution → Cleaning mode

In the spray execution state, motion generation queries the TF2 tree to produce surface aligned end-effector targets, and spray triggering is synchronized with robot motion. Low-level valve switching and safety interlocks are executed on the Arduino Portenta Machine Control via micro-ROS agent, decoupling deterministic actuation from higher-level perception or planning and reducing timing jitter in spray onset or offset which is critical for spray edge definition and repeatability. After completion of the job, AMSS can be transitioned into a cleaning mode, executing predefined flush sequences to reduce clogging risk and to stabilize response behaviour for subsequent material changes or restarts.

The implemented ROS 2 software architecture consists of distributed nodes for (1) perception (ToF acquisition + PBLPA), (2) TF2 frame publication (surface frame), (3) motion planning/control (surface-aligned trajectories), and (4) spray orchestration (state machine, parameter window handling, and command synchronization). The Portenta acts as a real-time hardware bridge through micro-ROS, providing services for valve switching, setpoint updates, and interlock status, while keeping safety-critical timing local to the embedded controller. Overall, this workflow forms a closed perception-to-actuation loop that supports material-specific multiple spraying mode while preserving modular integration across carriers.

4 Experimental evaluation

Experimental characterization evaluated the interaction of material rheology, spray modality, and AMSS actuation/control under reproducible conditions. This initial phase focuses on demonstrating multi-material sprayability with the same spray head and on showing that spray mode selection enables systematic changes in jet width and plume characteristics without hardware replacement.

4.1 Materials and rheological range

The investigated coating set represents typical flowable construction materials and covers a wide non-Newtonian viscosity spectrum. Since these coatings exhibit shear-thinning and, in some cases, thixotropy, viscosity values are reported as apparent (effective) viscosities derived from rotational viscometer measurements. As summarized in Table 2, the apparent viscosity range spans from 21.7 mPa·s (primer) up to 9247.6 mPa·s (surface filler/putty), including intermediate coatings to probe viscosity-driven sprayability trends.

Table 2. Apparent viscosity (effective) of the investigated non-Newtonian construction coatings.

Material	Apparent viscosity (mPa·s)
Primer (Caparol Rapidgrund)	21.7
Interior Latex Paint (Caparol Seidenlatex)	1200.5
Floor Coatings (Disbon 404 ELF 1K-Acryl-Bodensiegel)	1380.5
Exterior Façade Paint (Thermosan NQG)	2080.1
Roof Coatings (Disboroof 408 1K-Acryl-Dachfarbe)	2136.9
Surface Filler / Putty (Caparol Akkordspachtel SF Plus)	9247.6

4.2 Sprayability results and mode effects

To evaluate sprayability and identify stable operating conditions for each coating, the AMSS was tested using a material-specific, performance-based Design of Experiments (DOE). For each material introduced in Section 4.1, 40 trials were performed with systematic variation of spray mode, material pressure, pneumatic support, temperature, and nozzle orifice. The screening objective was to identify parameter regions that consistently produced a stable spray plume characterized by robust formation, symmetric fan development, and repeatable edges while remaining compatible with automated valve switching and perception-guided stand-off control.

Figure 5 shows the experimental setup used for these trials: (a) the Arduino Portenta Machine Control for deterministic valve actuation and interlocks, (b) the end-effector-mounted ToF camera integrated with the spray head for real-time stand-off and surface orientation estimation, and (c) automated spraying execution with AMSS. All experiments were conducted at a constant 300 mm stand-off, with run conditions defined by the DOE for each material–mode combination. High-speed imaging of the spray formation, at 2000 fps, was synchronized with AMSS process logs (spray mode, valve states, material and air pressure setpoints, temperature) to directly map the observed spray formation to the applied actuation configuration. Jet width in the reported frames in Fig. 6 is measured at the target plane using the in-frame calibration (≈ 32-34 px/cm). The results shown below (Fig. 6) are obtained using this integrated setup.

Figure 6 provides a compact visual summary of the results. Instead of showing every material, it presents a representative subset spanning the investigated range (primer → latex paint → floor coating → putty), demonstrating that stable spray formation is achievable

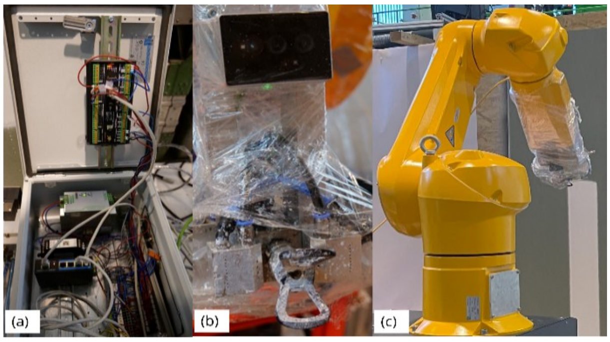

Figure 5. AMSS experimental setup: (a) Portenta Machine Control for valve actuation, (b) ToF camera for perception with spray head, and (c) automated spraying execution.

across substantially different material behaviours using the same modular spray head by appropriate selection of mode and parameter window. Across these runs, the observed plume widths fall in the range of 14-19 cm, indicating a consistent sprayability envelope at 300 mm stand-off over widely varying apparent viscosities.

Beyond sprayability, Fig. 6 and the paired runs show that spray mode selection can systematically modulate jet width even when major geometric and hardware factors are held constant (same material, nozzle orifice, pressure, temperature, and 300 mm stand-off). As summarized in Table 3, mode switching produced material-dependent changes in jet width. The associated full spray angles, estimated from (2 arctan $((\frac{w}{2}/d))$, change consistently with the measured widths, confirming that plume geometry is not solely pressure-driven and that spray modality provides an additional, embedded control dimension for coverage precision tuning without hardware replacement. In practice, this provides a process-level advantage for construction finishing: the spray pattern can be shifted between a wider fan for rapid area coverage and a narrower, more confined plume for

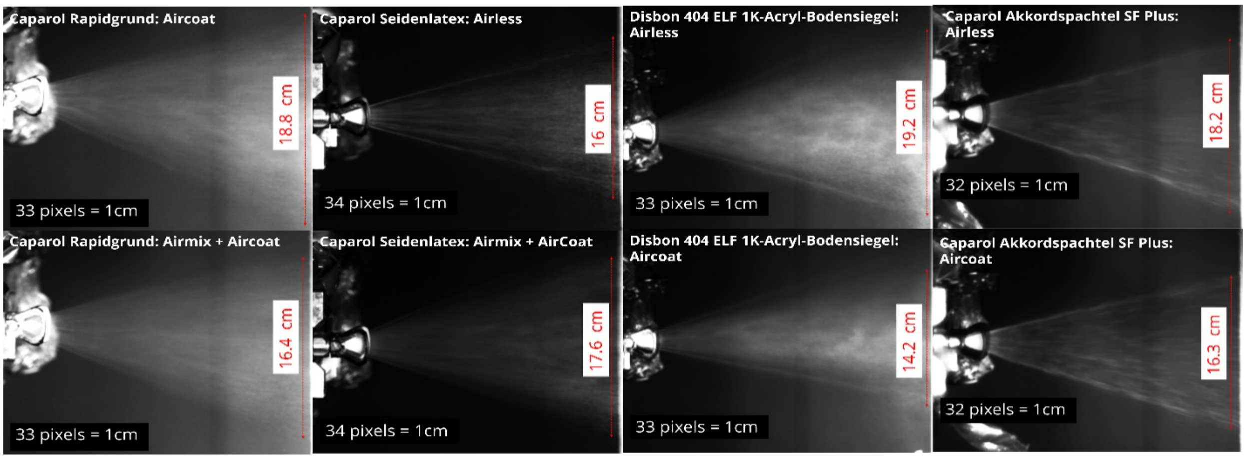

Figure 6. High-speed frames (2000 fps, 300 mm stand-off) showing mode-dependent jet-width modulation across representative construction coatings (calibrated at ≈32–34 px/cm).

edge-sensitive applications by changing only the spray mode. This supports the AMSS premise that the atomization strategy can be adapted in software/actuation rather than through nozzle or hardware replacement, while keeping the geometric boundary conditions constant.

In the present study, the primary baseline is defined as within system comparison between spray modes under otherwise fixed boundary conditions (material, nozzle, pressure, temperature, and stand-off), allowing the effect of spray modality to be isolated directly. Broader benchmarking against manual spraying and other robotic sprayers will require harmonized deposition metrics and comparable material–substrate conditions and is therefore part of future validation.

To complement the plume-based analysis, deposited-surface behaviour was quantified using pixel-based metrics extracted from the post-spray images. The detected spray area and its variation across runs were used as indicators of control over the deposited spray footprint, whereas edge overspray area relative to the sprayed area was used as an indicator of clean-edge spraying. Table 4 summarises these compact deposited-surface metrics together with the lowest edge-overspray condition identified for each material.

Table 3. Mode-dependent changes in jet width and implied spray angle at constant 300 mm stand-off, showing spray modality as a control lever under otherwise fixed conditions.

Material	Spray mode transition	Jet width (cm)	Δ width (cm)	Δ width (%)	Spray angle (°)
Primer	Aircoat → Airmix+Aircoat (60 bar, 40 °C, nozzle 327)	18.8 → 16.4	−2.4	−12.8%	34.8° → 30.6°
Interior latex paint	Airless → Airmix+Aircoat (100 bar, nozzle 321)	16.0 → 17.6	+1.6	+10.0%	29.9° → 32.7°
Floor Coatings	Airless → Aircoat (60 bar, nozzle 321)	19.2 → 14.2	−5.0	−26.0%	35.5° → 26.6°
Surface Filler / Putty	Airless → Aircoat (180 bar, nozzle 327)	18.2 → 16.3	−1.9	−10.4%	33.7° → 30.4°

5 Conclusion and Future Outlook

This paper adds to knowledge by showing that these challenges can be addressed at the end-effector level through the combination of multiple spray modes, deterministic valve-based actuation, and perception-guided stand-off and orientation control within one carrier-agnostic system. The results demonstrate stable sprayability across a wide apparent-viscosity range and show that spray mode selection provides an additional control dimension for modulating jet width under otherwise fixed boundary conditions, establishing a practical basis for future rheology-aware closed-loop spraying. AMSS combines a modular multi-mode spray head, valve-based actuation, and perception-driven pose regulation to support robotic spraying of materials with different rheological behaviour. Initial experiments demonstrate (1) multi-material sprayability across non-Newtonian construction coatings from low-viscosity primers to high-viscosity fillers using the same spray head, and (2) mode switching as an additional control lever that enables different jet widths and plume characteristics under identical baseline conditions. Integrated ToF-based perception with TF2 referencing further enabled automated control of stand-off distance and surface orientation, improving geometric consistency during execution. Beyond plume behaviour, pixel-based deposited-surface evaluation showed that the system can influence both the deposited spray footprint and the cleanliness of the spray boundary, as reflected by spray-area deviation and edge-overspray metrics.

Current limitations are practical and addressable: evaluation remains plume-focused, while deposited surface metrics, repeatability, and robustness under site-relevant disturbances have not yet been systematically quantified.

Table 4. Pixel-based deposited-surface metrics highlighting control over the deposited spray footprint and clean-edge spraying.

Material	Lowest edge-overspray condition	Spray area (mean ± SD, pixels)	Edge overspray area (% of spray, mean ± SD)
Interior paint	(Airless)	746,300 ± 13,165	8.06 ± 2.30
Floor coatings	(Airmix)	616,454 ± 46,376	3.50 ± 0.15
Roof coatings	(Airmix)	515,116 ± 18,564	2.01 ± 0.45
Exterior paints	(Airmix + Aircoat)	415,622 ± 41,817	4.79 ± 1.33
Surface filler	(Aircoat)	241,899 ± 18,790	4.35 ± 0.88

Future work will (i) add calibrated surface measurement to produce thickness maps and uniformity statistics, (ii) develop feedback-driven, rheology-aware selection of spray mode and setpoints within safe operating windows, and (iii) validate the system across representative site conditions and multiple carrier platforms to demonstrate transferable, construction-ready deployment.

Acknowledgements

This project was funded by the Federal Institute for Research on Building, Urban Affairs, and Spatial Development on behalf of the Federal Ministry for Housing, Urban Development, and Building with funds from the Zukunft Bau research funding program (funding code: 10.08.18.7-23.03).

References

[1] S. Rashidian, S. T. Hossain, K. Volz, and M. Teo. Enabling circularity in construction: A technology-phase alignment of construction 4.0 and circular economy principles. *Sustainable Production and Consumption*, 60:245–259, 2025.

[2] I. Kostavelis et al. RoBétArmé Project: Human-robot collaborative construction system for shotcrete digitization and automation through advanced perception, cognition, mobility and additive manufacturing skills. *Open Research Europe*, 4:4, 2024.

[3] Y. Wang, C. Mao, and T. Wang. Study of Human-Robot Collaborative Construction Task Allocation Problem Considering the Level of Task Danger. *Kalpa Publications in Computing*, 22:511-523, 2025.

[4] C. Okonkwo, A. Betancourt, S. Langar, and I. Awolusi. A BIM-Integrated Painting Approach in Construction with Autonomous Painting Robots. *EPiC Series in Built Environment*, 6:482-491, 2025.

[5] M. Menegaki and D. Damigos. A review on current situation and challenges of construction and demolition waste management. *Current Opinion in Green and Sustainable Chemistry*, 13:8–15, 2018.

[6] Q. Meng, Y. Zhao, P. Wang, and Y. Xiao. Development of a new spraying robot for building waterproof materials. *2nd International Conference on Cloud Computing and Mechatronic Engineering (I3CME 2022)*, pages 42, Chendu, China, 2022.

[7] E. Asadi, B. Li, and I.-M. Chen. Pictobot: A cooperative painting robot for interior finishing of industrial developments. *IEEE Robotics & Automation Magazine*, 25(2):82–94, 2018.

[8] Nanyang Technological University. OutoBot, an innovative robot to wash and paint high-rise buildings. On-line: https://phys.org/news/2017-03-outobot-robot-high-rise.html, Accessed: 03/12/2024.

[9] J. Chen. Overview of Automatic Spraying Technology for Building Exterior Walls. *JERA*, 9(1):100–105, 2025.

[10] M. Nakayama, S. Ishikawa, T. Nishiwaki, R. Oba, A. Kimura, and R. Tasaki. Skill-informed putty coating with a force-controlled robot arm on cast-like surfaces. In *2025 IEEE International Conference on Mechatronics and Automation (ICMA)*, pages 285–290, Beijing, China, 2025.

[11] HSE. Construction solvents: Spraying. On-line: https://www.hse.gov.uk/construction/healthrisks/hazardous-substances/spraying.htm, Accessed: 26/04/2024.

[12] M. Mlkvik, J. Jedelsky, H. P. Karbstein, and V. Gaukel. Spraying of viscous liquids: Influence of fluid-mixing mechanism on the performance of internal-mixing twin-fluid atomizers. *Applied Sciences*, 10(15):5249, 2020.

[13] C. Okonkwo and T. Sulbaran. A Review of Commercially Available Autonomous Painting Robots in the Construction Industry. In *Proceedings of 60th Annual Associated Schools of Construction International Conference*, pages 514–522, 2024.

[14] S. Poozesh, N. Akafuah, and K. Saito. Effects of automotive paint spray technology on the paint transfer efficiency – a review. *Proceedings of the Institution of Mechanical Engineers, Part D: Journal of Automobile Engineering*, 232(2):282–301, 2018.

[15] G. S. Settles, J. D. Miller, T. J. Hartranft, and A. D. Brandt. Visualization and collection of overspray from airless spray painting, 1998.

[16] Q. Ye, B. Shen, O. Tiedje, and J. Domnick. Numerical and experimental study of spray coating using air-assisted high-pressure atomizers. *Atomization and Sprays*, 25(8):643–656, 2015.

[17] O. N. Tursunovna. Technology of painting works in construction. On-line: https://doi.org/10.5281/ZENODO.7249088, Accessed: 01/10/2022.

[18] S. Neudecker et al. A New Robotic Spray Technology for Generative Manufacturing of Complex Concrete Structures Without Formwork. *Procedia CIRP*, 43:333–338, 2016.

[19] S. Ercan Jenny et al. Robotic plaster spraying: Crafting surfaces with adaptive thin-layer printing. *3D Printing and Additive Manufacturing*, 9(3):177–188, 2022.

[20] V. Frangez, E. Lloret-Fritschi, N. Taha, F. Gramazio, M. Kohler, and A. Wieser. Depth-camera-based rebar detection and digital reconstruction for robotic concrete spraying. *Construction Robotics*, vol. 5, 191–202, Dec. 2021.